WACCM simulations of the mean circulation and trace species transport in the winter mesosphere

Anne K. Smith,[1] Rolando R. Garcia,[1] Daniel R. Marsh,[1] and Jadwiga H. Richter[2]

Received 6 April 2011; revised 21 July 2011; accepted 23 July 2011; published 20 October 2011.

[1] Downwelling of air in the high latitude winter middle atmosphere causes perturbations in chemical composition. Species with sources in the mesosphere and lower thermosphere, such as nitric oxide and carbon monoxide, can be locally enhanced in the polar region. We investigate the origin of the downwelling air and the timescale for transport using the Whole Atmosphere Community Climate Model (WACCM). Analysis of the middle atmosphere transformed Eulerian mean (TEM) circulation, also called the residual circulation, is presented. This circulation gives the net air motion in the meridional and vertical directions due to the combined effects of the zonally averaged winds and the wave transport. The summer to winter circulation in the upper mesosphere during the solstice seasons includes strong upward motion at the summer pole and downward motion at the winter pole. During most winters, the air that is transported down by the circulation originates from low to middle latitudes in the upper mesosphere, 85–95 km; the timescale for this transport is 2–3 months. Trace species transport by molecular and eddy diffusion can bring high concentrations of thermospheric molecules into the winter mesosphere, where they are then brought to lower altitudes by the circulation. The magnitudes of the net tendencies due to advection by the TEM circulation and diffusion are similar. A case study of an active NH winter shows that the origin of the downwelling air in the TEM circulation is similar to that during average winters although the downwelling velocity is stronger by about a factor of two.

Citation: Smith, A. K., R. R. Garcia, D. R. Marsh, and J. H. Richter (2011), WACCM simulations of the mean circulation and trace species transport in the winter mesosphere, *J. Geophys. Res.*, *116*, D20115, doi:10.1029/2011JD016083.

1. Introduction

[2] Rapid downward transport of air into the middle atmosphere can cause significant perturbations to the chemical composition. *Randall et al.* [2006, 2009] demonstrated that downward transport of mesospheric or thermospheric NO into the stratosphere at the Northern Hemisphere (NH) winter pole led to a substantial enhancement in the destruction of stratospheric ozone. The degree of ozone destruction varied interannually depending on the dynamical variability and vortex stability in the middle atmosphere. The signature of downward transport during the NH winter of 2004 could also be seen in NO_2 [*López-Puertas et al.*, 2005; *Hauchecorne et al.*, 2007]. In the Southern Hemisphere (SH), the dynamical variations from year to year are appreciably smaller but the downward transport of NO can still be quite variable because the NO production varies. The evidence presented by *Randall et al.* [2007] indicates that the downward transport of NO in the SH depends primarily on the NO production by energetic particles in the mesosphere and lower thermosphere.

[3] Several studies have shown interannual variations in the downward transport into the NH winter middle atmosphere of other trace species that are more abundant in the thermosphere. *Smith et al.* [2009, 2010a] found strong variations in O around 85 km at the NH winter pole during the January-March period. Largest values were observed for 2004, 2006, and 2009, during the periods following the sudden stratospheric warmings of those years. Penetration of CO into the winter polar vortex was also seen in the 2004 winter [*Jin et al.*, 2005; *Funke et al.*, 2009]. *Damiani et al.* [2010] found OH perturbations in the northern high latitudes during the same periods; their analysis of simultaneous variations of OH and CO indicated that transport was responsible for the perturbations.

[4] An important process for the transport of trace species is the large-scale net motion of air. An example would be the displacement of air parcels from the thermosphere to the mesosphere or stratosphere. In order to be effective as transport, the timescale for the displacement must be short compared to the timescale for the air parcel to mix with the surrounding atmosphere or for the tracer to be created or destroyed by photochemical processes. The transformed Eulerian mean (TEM) circulation, introduced by *Andrews*

[1]Atmospheric Chemistry Division, National Center for Atmospheric Research, Boulder, Colorado, USA.
[2]Climate and Global Dynamics, National Center for Atmospheric Research, Boulder, Colorado, USA.

0148-0227/11/2011JD016083

and McIntyre [1976] closely approximates the net air parcel displacements in the latitude-pressure plane. The net mass motion associated with this circulation is an Eulerian representation of the zonally averaged Lagrangian motion due to the mean and perturbation winds. The TEM concept is valuable in diagnosing the net transport of trace species in the middle atmosphere.

[5] While the TEM circulation describes the bulk motion of large scale air masses, diffusive processes can change the concentrations of trace species within an air parcel. Eddy diffusion represents turbulent diffusion generated by wave breaking and is sometimes formulated to include transport of trace species by eddy flux divergence of organized gravity wave motion as well. The coefficient of diffusion is the same for all species although the actual diffusion rate depends on the vertical gradient of the species mixing ratio. Molecular diffusion is an important process for redistributing trace species at high altitudes as a result of the increased path lengths at low densities. Molecular diffusion acts to diffuse any trace species with a significant vertical gradient in mixing ratio and to impose a net vertical drift based on molecular mass. By these processes, chemical compounds that are generated in the thermosphere can be diffused into air parcels whose trajectories do not cross above the mesopause.

[6] This paper uses multiyear simulations from the Whole Atmosphere Community Climate Model (WACCM) to determine the transport processes in the mesosphere lower thermosphere (MLT) region. The separate contributions from these processes to the distributions of several trace species are presented. The species that we focus on are CO_2, CO, O, and NO. The results show the mean circulation, its impact on the mean distributions, and the role of eddy and molecular diffusion. Trajectories of the air parcel advection by the TEM circulation show the typical path of air that descends over the winter poles. One case study follows the circulation and evolution of trace species during a dynamically active NH winter. The discussion explains how the total number of molecules limits the impact that large-scale transport of thermospheric air can have on the middle atmosphere.

2. WACCM: Whole Atmosphere Community Climate Model

[7] The Whole Atmosphere Community Climate Model, WACCM, is a high-top model based on the NCAR Community Climate System Model. WACCM is an optional variation of the Community Atmosphere Model (CAM) that has been designed to investigate the interactions of chemistry, radiation, and dynamics and their impact on the Earth's climate system. The atmospheric component of WACCM extends from the Earth's surface to 5.96×10^{-6} hPa.

[8] The current study uses WACCM version 3.5, which uses the physics suite from CAM3.5 [*Gent et al.*, 2009]. *Garcia et al.* [2007] give a detailed description of an earlier version of WACCM. *Marsh et al.* [2007] describe the energetics and solar forcing. Updates are described in *Richter et al.* [2010]. The present integrations have a horizontal resolution of 2.5° in longitude and 1.9° in latitude. There are 66 vertical levels; vertical resolution is about 1.25 km in the lower stratosphere, decreases to 1.75 km in the upper stratosphere, and 3.5 km above 65 km. The time step is 30 minutes.

[9] Four WACCM integrations beginning in 1953 and extending through 2006 were carried out as part of a suite of simulations made in support of the Chemistry Climate Model Validation (CCMVal) program [*Eyring et al.*, 2006]. In all of these integrations, model values for sea surface temperatures, anthropogenic and natural surface gas emissions, volcanic aerosols, solar flux, geomagnetic activity, and momentum forcing for the parameterized QBO were specified from observations. With slight differences in the initial conditions, the four different realizations produce different weather patterns. Since WACCM is a free-running model, weather in the model diverges from the observations for a particular day. Monthly and annual mean values do not necessarily correspond to the equivalent years in the atmosphere.

3. Analysis

[10] WACCM output data are available monthly; the files represent the average over every time step during the month. Unless otherwise noted, these monthly mean fields are used here. A limited number of dynamical fields are available as daily averages and are used where higher time resolution is required. These output products do not allow the separation of daytime and nighttime data for trace chemical species that have different concentrations during day and night. However, the species we consider have long lifetimes over the part of the domain of interest. Therefore the averaging of day and night data does not adversely affect the analysis.

[11] The continuity equation for the mixing ratio μ of a tracer is given by

$$\frac{d\mu}{dt} = P - L\mu + X_K + X_D \tag{1}$$

where

$$\frac{d}{dt} = \frac{\partial}{\partial t} + \frac{u}{a\cos\phi}\frac{\partial}{\partial\lambda} + \frac{v}{a}\frac{\partial}{\partial\phi} + w\frac{\partial}{\partial z}. \tag{2}$$

t is time, λ is longitude, ϕ is latitude, z is the vertical coordinate (see below), and u, v, and w are the vector components of the wind. P is the photochemical production rate and L is the photochemical loss rate. X_K and X_D are the chemical tendencies due to eddy and molecular diffusion, respectively. Eddy diffusion is a parameterization of processes that mix air parcels in the vertical but that are not resolved by the model (e.g. gravity wave flux divergence, turbulent mixing). It is given by

$$X_K = \frac{1}{\rho_0}\frac{\partial}{\partial z}\left(\rho_0 K_{zz}\frac{\partial\mu}{\partial z}\right) \tag{3}$$

The eddy diffusion coefficient K_{zz} is a product of the gravity wave parameterization in the model. See *Garcia et al.* [2007] and *Richter et al.* [2010] for a description of the gravity wave parameterization in WACCM.

[12] The vertical coordinate used in the analysis, z, is the log-pressure altitude, defined by $z = -H_0\log(p/p_s)$ where H_0 is a constant approximate scale height of 7 km and p_s is the mean surface pressure. z is an isobaric coordinate and, in general, differs from the geometric altitude. For comparison with observations, the figures and discussion in this paper indicate the annual global average geometric height for a given WACCM pressure level.

[13] For molecular diffusion, WACCM uses the parameterization of *Banks and Kockarts* [1973], which treats the diffusion of a minor trace species through a background atmosphere composed of the dominant species (N_2, O_2, O). This is a valid approximation throughout the range of altitudes spanned by WACCM. X_D is given by

$$X_D = \frac{1}{\rho_0}\frac{\partial}{\partial z}\left\{\rho_0 D_\mu\left[\frac{\partial \mu}{\partial z} - \frac{\mu}{H}\left(1 - \frac{H}{H_\mu}\right)\right]\right\}. \quad (4)$$

where H is the scale height of the background atmosphere, $H = (kT)/(Mg)$, k is Boltzmann's constant, g is the acceleration of gravity, and M is the mean molecular mass of the atmosphere in atomic mass units. Likewise, H_μ is the scale height of μ, given by $H_\mu = (kT)/(M_\mu g)$. It is evident from equation (4) that molecular diffusion includes a diffusive term that depends on the mixing ratio gradient and is analogous to the eddy diffusion. It also includes a contribution from the relative mass. Equation (4) can be written as

$$X_D = \frac{1}{\rho_0}\frac{\partial}{\partial z}\left(\rho_0 D_\mu \frac{\partial \mu}{\partial z}\right) - \frac{1}{\rho_0}\frac{\partial}{\partial z}(\rho_0 \mu w_D). \quad (5)$$

where

$$w_D = \frac{D_\mu}{H}\left(1 - \frac{H}{H_\mu}\right). \quad (6)$$

w_D is the "diffusive separation velocity". The sense of w_D is such that molecules that are heavier than the background atmosphere (i.e., those with molecular mass greater than 28.97 atomic mass units) are displaced downward while those that are lighter are displaced upward.

[14] The magnitudes of both the diffusive and advective molecular diffusion tendencies depend on the coefficient D_μ [*Banks and Kockarts*, 1973]. D_μ in units of $m^2\ s^{-1}$ is given in equation (7) for M and M_μ in atomic mass units, T in K and n in m^{-3}.

$$D_\mu = 1.52 \times 10^{20}\left(\frac{1}{M_\mu} + \frac{1}{M}\right)^{1/2}\frac{T^{1/2}}{n} \quad (7)$$

D_μ increases with temperature, an effect that is enhanced because of the dependence of the background number density n on T. Also note that the magnitude of D_μ is largest for species with low mass.

[15] To write equation (1) in the TEM system, we separate all the model-resolved fields into zonally averaged and perturbation components ($\mu = \overline{\mu} + \mu'$). The equation for the zonal mean budget of $\overline{\mu}$ is

$$\frac{\partial \overline{\mu}}{\partial t} + \frac{\overline{v}}{a}\frac{\partial \overline{\mu}}{\partial \phi} + \overline{w}\frac{\partial \overline{\mu}}{\partial z} + \frac{1}{a\cos\phi}\frac{\partial \overline{v'\mu'}\cos\phi}{\partial \phi} + \frac{1}{\rho_0}\frac{\partial \rho_0 \overline{w'\mu'}}{\partial z} = \overline{P} - \overline{L}\overline{\mu} - \overline{L'\mu'} + \overline{X_K} + \overline{X_D} \quad (8)$$

[16] The TEM meridional and vertical winds, $\overline{v}^*$ and $\overline{w}^*$, are defined as [*Andrews and McIntyre*, 1976]

$$\overline{v}^* \equiv \overline{v} - \frac{1}{\rho_0}\frac{\partial}{\partial z}\left(\rho_0 \frac{\overline{v'\theta'}}{\overline{\theta}_z}\right) \quad (9)$$

$$\overline{w}^* \equiv \overline{w} + \frac{1}{a\cos\phi}\frac{\partial}{\partial \phi}\left(\cos\phi \frac{\overline{v'\theta'}}{\overline{\theta}_z}\right) \quad (10)$$

The definitions for $\overline{v}^*$ and $\overline{v}^*$ are substituted into equation (8), which then becomes

$$\frac{\partial \overline{\mu}}{\partial t} + \frac{\overline{v}^*}{a}\frac{\partial \overline{\mu}}{\partial \phi} + \overline{w}^*\frac{\partial \overline{\mu}}{\partial z} = \overline{P} - \overline{L}\overline{\mu} - \overline{L'\mu'} + \overline{X_K} + \overline{X_D} + F. \quad (11)$$

The term F denotes the TEM divergences of wave fluxes,

$$F = \frac{1}{a\cos\phi}\frac{\partial}{\partial \phi}\left[\cos\phi\left(\overline{v'\mu'} - \frac{\overline{\mu}_\phi}{a\overline{\theta}_z}\overline{v'\theta'}\right)\right] - \frac{1}{\rho_0}\frac{\partial}{\partial z}\left[\rho_0\left(\overline{w'\mu'} + \frac{\overline{\mu}_z}{\overline{\theta}_z}\overline{v'\theta'}\right)\right] \quad (12)$$

The wave flux divergence terms (equation (12)) represent the effective transport of trace species when the gradient or chemical lifetime varies over the path length of resolved wave structures. This can be important for planetary waves in the stratosphere [*Garcia and Solomon*, 1983] and lower mesosphere [*Siskind et al.*, 1997] but is negligible in the upper mesosphere where vertical eddy transport is due to small scale gravity waves. The small scale gravity waves are not simulated explicitly in WACCM. Instead, eddy transport by gravity waves is parameterized by the term X_K. F also can be important for vertical transport of atomic oxygen by the diurnal tide near the equator, but this is outside of the region of interest for this paper. Therefore, in what follows, we ignore F in equation (11).

[17] In this paper we examine the mean and interannual variability of the transport and diffusion terms: $\overline{v}^*$, $\overline{w}^*$, X_D, and X_K and their impacts on four trace species in the upper mesosphere. The emphasis is on the downward transport into the high latitude mesosphere of chemical species produced in the MLT during winter.

4. Climatological Circulation and Transport

[18] Simulation of the stratospheric climate and composition by WACCM has been compared with observations and with other models by *Eyring et al.* [2010] and *World Meteorological Organization* [2010]. The model performs well in the stratosphere, where there are numerous observations available for validation. Due to much less available data above 50 km, there has not been a thorough evaluation of the model simulations of the mesosphere. Selected comparisons of temperature and zonal winds [*Garcia et al.*, 2007; *Richter et al.*, 2010] indicate that the model climatology compares well with available global satellite observations.

[19] There were significant changes in the composition of the atmosphere over the period used in this study (1960–2005). Most important are the increase in CO_2 and in halogen species that accelerate the destruction of ozone. As shown by *Smith et al.* [2010b], the model predicts large trends in the mesospheric circulation at high southern latitudes during the summer months. Trends in winter (both hemispheres) were smaller and were not consistent among the four model realizations analyzed here. The small and inconsistent trends in the winter mesospheric circulation are not considered further in this paper.

[20] The climatological circulation and trace species distributions include data from all months between January 1960 and December 2006 of the four realizations. The climatology for each calendar month therefore includes monthly averages from 188 model years.

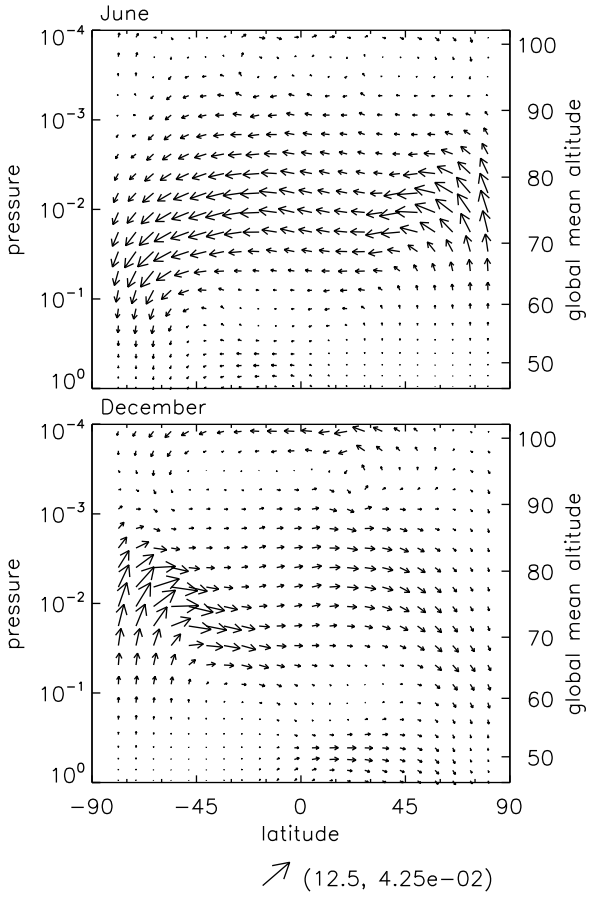

Figure 1. Vectors showing the WACCM climatological TEM flow for June and December averaged over 1960–2006 for four model realizations. The scale at the lower right shows the maximum $\overline{v}^*$ and $\overline{w}^*$ in m/s. For reference, the right axis on all figures gives the climatological global mean geometric altitude from WACCM.

4.1. TEM Velocities

[21] Figure 1 shows a vector representation of the WACCM climatological TEM velocity for the solstice months of June and December in the MLT region. The pattern shows two circulation cells: upward in summer and downward in winter below about 90 km (geometric altitude) and upward in winter and downward in summer above the same altitude. The strongest vertical velocity is the upwelling in the summer high latitudes that is responsible for the cold summer mesopause. To illustrate the displacements associated with the velocity vectors, note that meridional velocity of 1 m/s corresponds to 2.57 degrees of latitude per day and vertical velocity of 0.01 m/s corresponds to 1.16 km/day. For the solstice periods, the mean velocities in the MLT can be as large as 10 degrees of latitude and 5 km in the vertical per day.

[22] Both the winter and summer circulation are stronger in the SH although the differences are much more pronounced in winter. *Smith et al.* [2010b] discuss the hemispheric differences in the TEM circulations during the late spring and early summer. The hemispheric differences during both seasons result from differences in the gravity wave forcing of the circulation in WACCM (Figure 2). Stratospheric winds filter upward propagating gravity waves and therefore can have a strong impact on the driving of the MLT circulation, which is due in large part to breaking or dissipating gravity waves. The stronger jet in the SH stratosphere leads to a greater disparity between eastward and westward gravity wave fluxes and ultimately to stronger circulation driving than in the NH. *Siskind et al.* [2003] reported a stronger gravity wave driven circulation in July than in January in simulations using a two-dimensional model, consistent with the WACCM results for those months (not shown). Note that the weak NH gravity wave forcing climatology also includes the effects of sudden stratospheric warmings, which occur in about 60% of winters in these simulations. Even though the NH gravity wave drag appears to be weak in the December average in WACCM, the simulated mean winds are realistic [*Richter et al.*, 2010].

[23] The TEM velocity can also be written in terms of a stream function χ^*, defined by

$$\overline{v}^* = -\frac{1}{\rho_0 \cos\phi}\left(\frac{\partial \rho_0 \chi^*}{\partial z}\right) \tag{13}$$

$$\overline{w}^* = \frac{1}{a\cos\phi}\frac{\partial \chi^*}{\partial \phi} \tag{14}$$

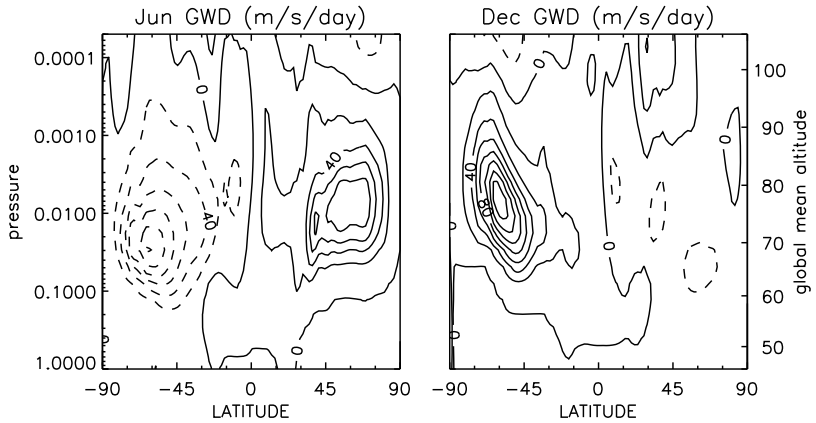

Figure 2. WACCM climatological gravity wave drag for June and December averaged over 1960–2005 for four model realizations. Units are m/s/day.

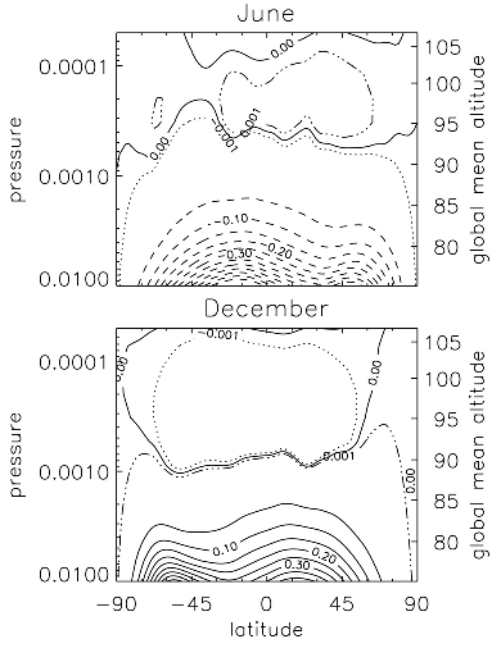

Figure 3. Contours of the WACCM climatological TEM mass stream function for June and December averaged over 1960–2005 for four model realizations. Contour interval is 0.05. The dot and dot-dash contours are for −0.001 and 0.001, respectively. Units are m^2/s.

The stream function for the mean June and December TEM is calculated by integrating equation (14) (Figure 3). The circulation is more vigorous where the stream function lines are closer together. To the extent that these mean streamlines represent the conditions for an extended period, they may be used to visualize the net trajectories of air parcels. The only way to move conserved trace species across the streamlines is by eddy or molecular diffusion. In addition, trace species can be changed along the streamlines by photochemistry (the term $\overline{P} - \overline{L}\overline{\mu} - \overline{L'\mu'}$ in equation (11)).

[24] From Figures 1 and 3 it is evident that the altitude of the transition from the lower (poleward and downward) circulation cell to the upper (poleward and upward) cell is somewhat different in June and December. In the December mean, the transition occurs around 0.001 hPa. In the June mean, the transition occurs around 0.0005 hPa, higher by ~3 km. This is primarily due to the differences in gravity wave driving of the circulation associated with hemispheric differences in the filtering of gravity waves by stratospheric zonal winds.

[25] *Lieberman et al.* [2000] derived the TEM circulation as a residual to balance the diabatic heating determined from temperatures measured by the High Resolution Doppler Imager (HRDI) on the Upper Atmosphere Research Satellite. They also compared the calculated meridional TEM winds ($\overline{v}^*$) with the meridional winds ($\overline{v}$) measured by HRDI and with mean solstice winds measured by several radar techniques at a range of latitudes. No consistent agreement between the calculated $\overline{v}^*$ and the measured winds was found. The altitude where the HRDI $\overline{v}^*$ reached its maximum magnitude was near or above 100 km for both solstice seasons, much higher than in the WACCM simulations (Figure 1). In the summer hemisphere, the circulation computed by *Lieberman et al.* [2000] changed from upward to downward around 95 km, in good agreement with the WACCM results. However, in the winter, they calculated downward motion from HRDI through the entire domain of the analysis (60–105 km) whereas the WACCM simulations indicate a turnaround at about 95 km.

[26] Due to the difficulty of determining the global circulation in the MLT region, we expect that a definitive validation cannot be made by comparing the WACCM simulated winds with observational analyses. A more fruitful path for determining the strength and structure of the mean circulation is likely to be found by comparing the distributions of advected tracers. The strong seasonal and latitudinal variations in the WACCM simulations of some tracers, shown and discussed in section 4.3, provide a robust signal for validation.

4.2. Eddy and Molecular Diffusion

[27] The eddy diffusion coefficient in WACCM is a product of the gravity wave drag parameterization. See *Garcia et al.* [2007] and *Richter et al.* [2010] for descriptions of the parameterization. The gravity wave sources used in the model are not specified uniformly. Instead, the sources are tied to convection (predominantly in the tropics) and the presence of fronts (predominantly in middle and high latitudes). The diffusion coefficient is proportional to the gravity wave drag and inversely proportional to the effective Prandtl number (*Pr*). *Pr* is used for the diffusion of heat as well as for trace species so it can also affect the energy balance [*Huang and Smith*, 1991]. *Pr* is set to 4 in the results presented here. This value was chosen to give a good match between the WACCM simulations and the measured profiles of CO_2 [*López Puertas et al.*, 2000; *Beagley et al.*, 2010].

[28] As shown in equation (5), the effect of molecular diffusion on a trace species can be expressed as the sum of two different contributions. One part has the form of diffusion (i.e., the tendency is proportional to the second derivative of the species mixing ratio). The other contribution has the form of advection (i.e., the tendency depends on a "velocity" and the vertical gradient of the species mixing ratio). Both the diffusion coefficients and the effective drift velocity are different for each chemical species.

[29] The tendencies of trace species due to both molecular and eddy diffusion depend on the vertical gradient of the species (equation (11)) and on the diffusion coefficients. Figure 4 compares the diffusive part of molecular diffusion (Figure 4b) with the eddy diffusion coefficient (Figure 4a) for December. The eddy diffusion varies strongly with latitude as a result of the distribution of gravity wave sources and the filtering of gravity waves by middle atmosphere winds. Note that there is a peak in the eddy diffusion coefficient for the NH even though the gravity wave drag (Figure 2) is small. The parameterized effects from dissipating eastward and westward waves cancel to reduce the magnitude of the drag but sum to give a peak in the diffusion coefficient.

[30] The molecular diffusion coefficient for a particular species varies only with temperature and density and is therefore fairly uniform in latitude and steady in time. The rate is higher for species with lower atomic weight (see

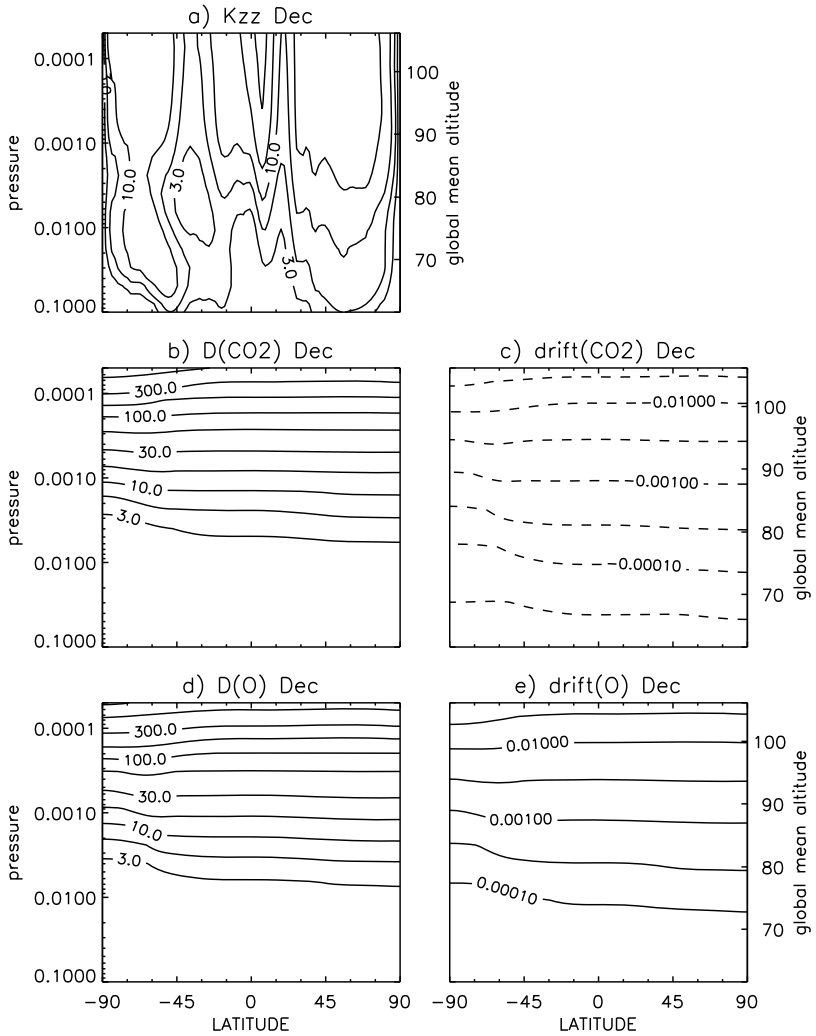

Figure 4. Latitude × pressure cross-sections of WACCM climatological values for diffusion during December: (a) eddy diffusion coefficient (K_{zz}) (b) molecular diffusion coefficient for CO_2 (D_{CO2}); (c) effective molecular drift velocity w_D for CO_2 (d) molecular diffusion coefficient for O (D_O); (e) effective molecular drift velocity w_D for O. Units are m^2/s for Figures 4a, 4b, and 4d; units are m/s for Figures 4c and 4e.

equation (7)). The other part of molecular diffusion, the vertical drift of a species relative to the background atmosphere, can be either positive or negative. The sign depends on the molecular mass of the species relative to the molecular mass of the background atmosphere. In WACCM, the molecular mass of the atmosphere is kept constant at 28.97 atomic mass units. Figure 4 shows the effective vertical drift velocity for O (16 amu) and CO_2 (44 amu). The magnitudes of w_D are smaller by about a factor of 10 for CO and NO (not shown), whose molecular masses (~28 and ~30, respectively) are very close to the mass of the background atmosphere. The net impacts of molecular and eddy diffusion on tracer tendencies are compared to the impacts of advection by the TEM circulation in section 4.3.

4.3. Trace Species Distributions and Transport Tendencies

[31] We can reconstruct the transport terms in equation (11) for the trace species in the middle atmosphere from WACCM. Using CO, CO_2, NO, and O as examples, we determine the contributions to the zonal mean budget in the upper mesosphere. CO_2 is destroyed by photolysis and chemical loss in the thermosphere. Its mixing ratio has a negative vertical gradient due primarily to this loss. The vertical gradient of mixing ratio is also affected by molecular diffusion [*LópezPuertas et al.*, 2000] and by the positive trend in emissions from the Earth's surface. CO is produced by the destruction of CO_2; its vertical gradient is positive in the MLT region. CO can also be produced by the oxidation of CH_4; this source is important in the stratosphere and lower mesosphere but does not have much of an impact on the CO concentration in the MLT [*Minschwaner et al.*, 2010]. The CO concentrations in the thermosphere are likely underestimated in these model simulations due to a neglect of CO_2 photolysis at extreme ultraviolet (EUV) wavelengths and of the reaction of CO_2 with the O^+ ion. These additional sources of CO (to be included in future model runs) affect the thermospheric CO concentration but

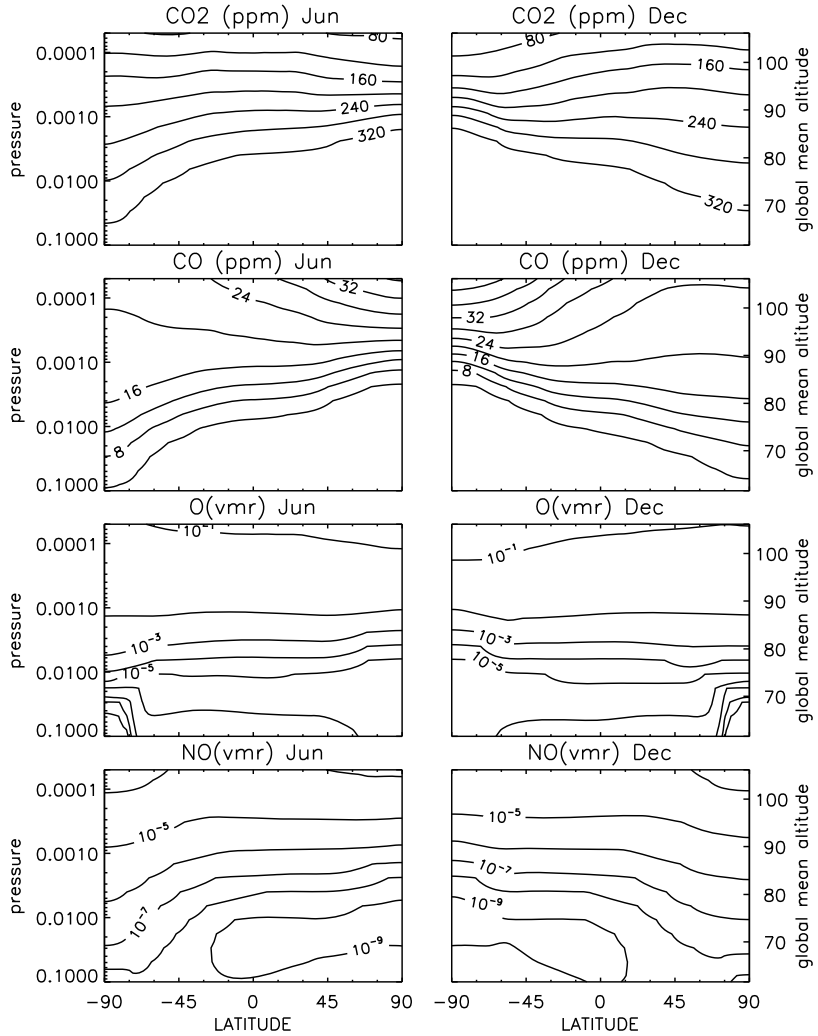

Figure 5. WACCM climatological mixing ratios of CO, CO_2, O, and NO during December and June. Units are ppmv for CO and CO_2, plotted with linear contour intervals. Units are mixing ratio for O and NO, plotted with logarithmic contour intervals.

have little impact below the mesopause. O is abundant and long-lived in the thermosphere. Due to sharp changes in the production rate and the photochemical lifetime, the O mixing ratio has a very strong positive gradient in the upper mesosphere. NO is produced in the auroral zones and also as a byproduct of ionizing EUV radiation. *Marsh et al.* [2007] show the horizontal and vertical distributions of the NO production in the MLT simulated by WACCM.

[32] Figure 5 shows the average distributions of these four species in December and June. The distributions reflect the mean circulation shown in Figure 1. CO and CO_2 have long lifetimes in the MLT and behave like tracers on a seasonal timescale. Upwelling in the summer mesosphere is associated with high concentrations of CO_2 and low concentrations of CO. Downwelling in the winter has the opposite effect. The mixing ratios of CO and CO_2 also respond to the oppositely directed vertical velocities in the polar regions above 90–95 km. As a result of the converging vertical winds above the summer mesopause, the vertical gradients of CO and CO_2 are strongest there.

[33] Most of the carbon in the MLT is tied up in either CO_2 or CO; the balance changes due to photochemical reactions. It is evident from Figure 5 that the sum of these two species is not constant. There are two reasons for this. 1) Molecular diffusive drift has a strong impact on redistributing CO_2 and a lesser impact on CO so this process keeps the molecules out of balance. 2) Due to multiyear transport times, there are gradients in both molecules that result from the strong trend in CO_2 emissions at the Earth's surface.

[34] In the upper mesosphere (70–95 km), the distribution of NO has a pattern that is similar to that of CO; the patterns diverge below 70 km due to different chemical sources. This distribution indicates that downwelling of NO-rich air near the winter pole and upwelling of NO poor air near the summer pole impacts the global distribution [*Marsh and Roble*, 2002]. Above 95 km, the NO distribution differs from that of CO. NO still has a positive gradient in the vertical direction but the NO distribution in the thermosphere does not show any indication that transport by the

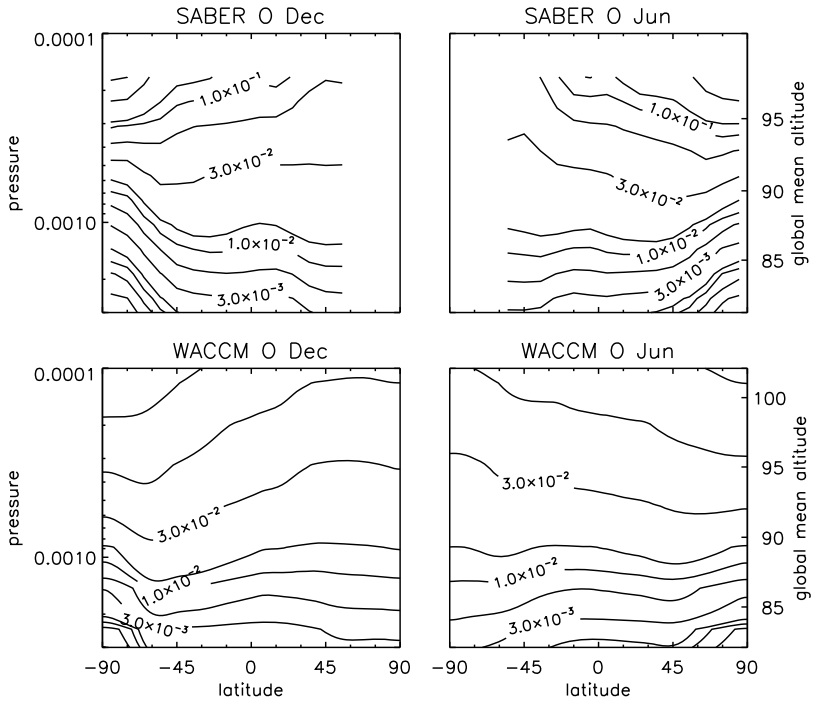

Figure 6. Climatological mixing ratio of atomic oxygen from (top) SABER (2002–2010) and (bottom) WACCM for December and June.

circulation cell above the mesopause (rising motion near the winter pole) is controlling the distribution. The NO maximum at the winter pole in the altitude range 95–110 km shows the impact of production in the auroral zones and loss triggered by NO photolysis [*Marsh*, 2011]. For the altitude range shown in Figure 5, the distribution of NO_x is almost identical to that of NO.

[35] Where its lifetime is long, above about 85 km, the distribution of O also responds to transport by the mean circulation. Like CO and CO_2, it has strongest vertical gradients at the summer pole at the altitude where the upwelling and downwelling cells meet. Below 80 km, the lifetime of O is short and its distribution is strongly affected by photochemistry. The extremely low values near the winter pole indicate a low concentration of O during the continuous darkness of polar night.

[36] The troposphere and stratospheric sources and mesosphere photochemical loss give an overall negative gradient with altitude for water above about 60–70 km. Therefore, upwelling at a particular latitude in the MLT region will increase the water concentration while downwelling will decrease it. The chemical loss rate is slow so transport on a seasonal timescale affects the water distribution. Transport causes the maximum water at high latitudes to occur during the season with upwelling motion.

[37] Seasonal distributions of H_2O in polar latitudes from Odin satellite measurements were compared with WACCM simulations by *Lossow et al.* [2009]. The patterns are quite similar. In both cases, there is a summer maximum in water near 70–80 km, due to summer upwelling, and there is a winter maximum above 100 km, due to winter upwelling. One way to evaluate the model performance in the two hemispheres is to compare the altitude at which the seasonal maximum in water changes from summer to winter. In the SH, both the Odin observations and WACCM simulations have this transition at about 92 km; i.e., below 92 km, the annual maximum in water occurs during summer and above 92 km the annual maximum occurs during winter. This seasonal distribution is determined mainly by vertical transport and so it is a good proxy for upwelling. The water maxima seen in Odin during the winter at high altitudes are an excellent confirmation that the mean circulation has reversed near the mesopause. However, in the NH, the altitude of the transition to winter maximum is lower in WACCM (~90 km) than in the Odin observations (~95 km). The WACCM simulations analyzed in this study did not include polar mesospheric clouds (PMC). Condensation, settling, and evaporation associated with PMC can redistribute water in the summer upper mesosphere; neglect of these processes may contribute to discrepancies between the simulations and observations.

[38] A similar discrepancy is seen in the distribution of O in the winter hemisphere as simulated by WACCM and measured by SABER (Figure 6). See *Smith et al.* [2010a] for a description of the determination of O from SABER. Due to the instrument viewing direction, SABER observations extend only to 53° in the winter hemisphere. In June, the contours of constant O mixing ratio slope upward from SH to NH at 85 km and slope downward at 95 km. The slope indicates downwelling in the winter mesosphere (southern middle to high latitudes) and upwelling at higher altitudes. The transition between upward sloping and downward sloping contours can give an estimate about the altitude where the circulation changes from downwelling to upwelling. The June SH transition levels are at about 0.0008 hPa in both model and observations. However, for NH December,

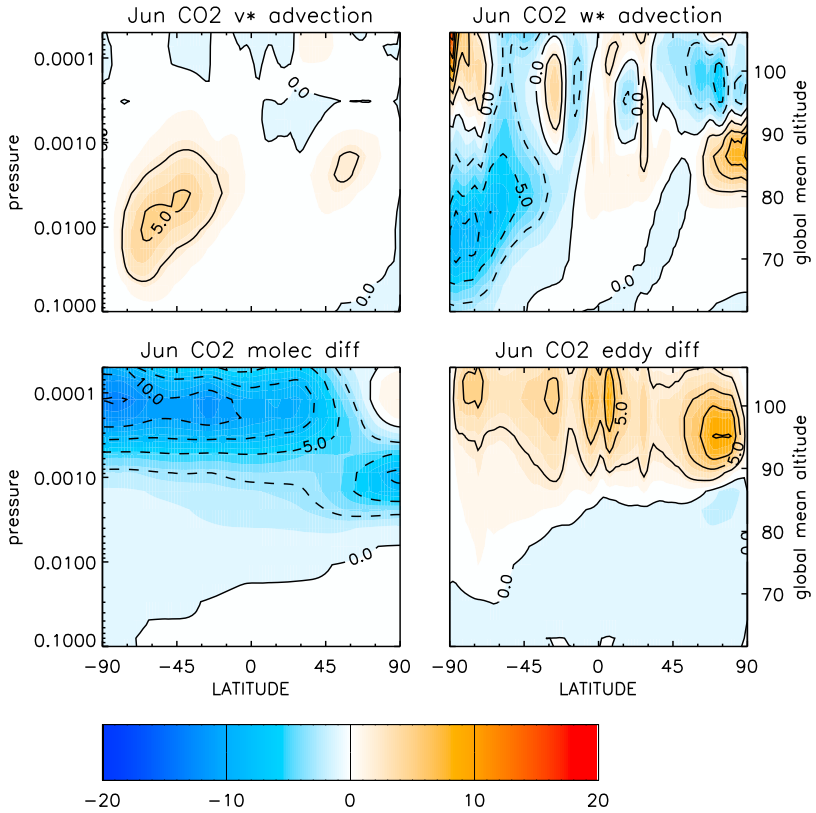

Figure 7. Climatological WACCM tendency of CO_2 due to advection by the TEM meridional velocity, the TEM vertical velocity, molecular diffusion, and eddy diffusion during June. Units are ppmv/day.

the levels are ~0.0008 hPa for WACCM and ~0.0005 hPa for SABER.

[39] The H_2O and O measurement comparisons with WACCM confirm the basic direction of the circulation in the MLT. However, the comparisons also indicate that the altitude of the upward circulation cell in the NH winter is too low in WACCM. This indicates that the altitude of strong poleward motion in the model is too low during NH winter. (Due to continuity, the transition from downwelling to upwelling flow depends on the vertical and meridional structure of $\overline{v}^*$.) In WACCM, the altitude of the poleward winter flow is controlled by the gravity wave parameterization. In particular, it is the altitude of the maximum momentum deposition of breaking gravity waves. The discrepancies suggest that the breaking level for gravity waves in the NH winter in the WACCM parameterization is too low. The breaking level depends on parameters in the gravity wave parameterization, particularly the assumed wave amplitude at the source level (in the troposphere). This discrepancy is being further investigated.

[40] Figure 7 shows the tendencies of WACCM CO_2 due to meridional and vertical advection by the TEM circulation, molecular diffusion, and eddy diffusion for June. The tendencies of CO_2 in response to the net drift component of molecular diffusion is negative. The effective molecular diffusion velocity w_D is downward for CO_2. Since the gradient is negative (Figure 5), this leads to a negative tendency. From the magnitudes of the tendencies in Figure 7, it is evident that the primary transport tendencies for CO_2 in WACCM around the time of solstice are due to the vertical advection by the TEM and the molecular drift. Eddy diffusion is variable in space but can be locally dominant.

[41] Figure 8 shows the December tendencies of the four species shown in Figure 5. The tendency terms at each pressure level are expressed as a percentage of global mean concentration at that level. For example, a value of 200% (as for the NO tendency due to advection by the TEM circulation at the winter pole at 0.01 hPa) means that the tendency is to increase the NO concentration daily by an amount that is double the global average concentration at 0.01 hPa. For CO, O and NO, the strongest magnitudes occur in the winter high latitudes around 65–90 km (0.1–0.001 hPa). This reflects the dynamical processes that are transporting concentrations far in excess of the global mean mixing ratios at this altitude. It is also evident that the tendencies due to the vertical eddy and molecular diffusion can, in some regions, be larger than those due to the TEM circulation. Downward transport of trace species into the winter pole will result from the net effect of air parcel advection by the TEM circulation and movement of trace species into or out of air parcels by diffusion. The tendencies for June (not shown) have maxima in the opposite hemisphere; the patterns are very similar although the magnitudes of the tendencies due to the TEM advection are larger by about a factor of two. Since the tendencies due to diffusion have similar magnitudes in the two hemispheres, the net effect is a stronger transport of tracers in the SH winter than in the NH.

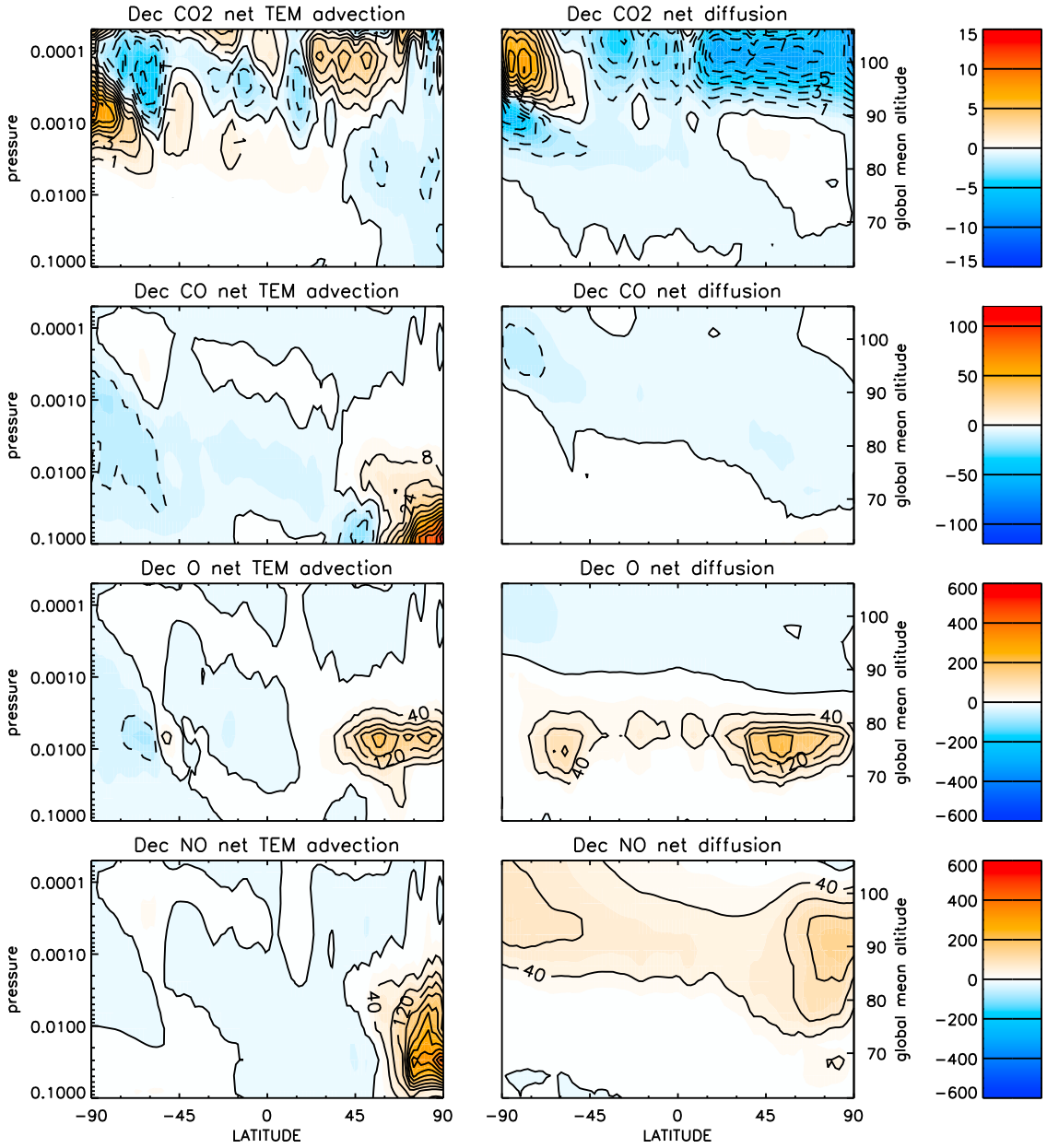

Figure 8. Climatological mixing ratio tendencies for CO_2, CO, O and NO during December due (left) to the TEM circulation and (right) to the sum of eddy and molecular diffusion. Units are change in mixing ratio as a percent of the long term mean mixing ratio over all latitudes and months at each pressure level. Contour intervals are 1% for CO_2, 8% for CO, and 40% for O and NO.

4.4. Trajectories and Timescales of Air That Is Advected to the Winter Pole

[42] There is increasing evidence that CO, O, and NO, which have sources in the upper mesosphere that increase into the thermosphere, are on occasion transported into the mesosphere and stratosphere. NO has received a lot of attention because, when it penetrates into the middle stratosphere or lower, it can lead to significant enhancement in the destruction of stratospheric ozone [*Randall et al.*, 2006, 2007, 2009; *Hauchecorne et al.*, 2007].

[43] O is also very important for ozone since it is one of the species needed for production. In the part of the atmosphere where its lifetime is long (above about 80 km and at even lower altitudes in the polar night), its distribution and variability are strongly affected by transport on timescales of hours to months [*Smith et al.*, 2010a]. Ozone is short-lived in the mesosphere and its concentration is directly related to the production rate through the reaction of O with O_2. Transport of O therefore directly affects the amount of mesospheric ozone, including the ozone values at the secondary maximum (90–95 km) [*Smith and Marsh*, 2005].

[44] The production of CO ceases in the darkness of polar night but its loss continues in the MLT where OH is present during night [*Minschwaner et al.*, 2010]. From the observed

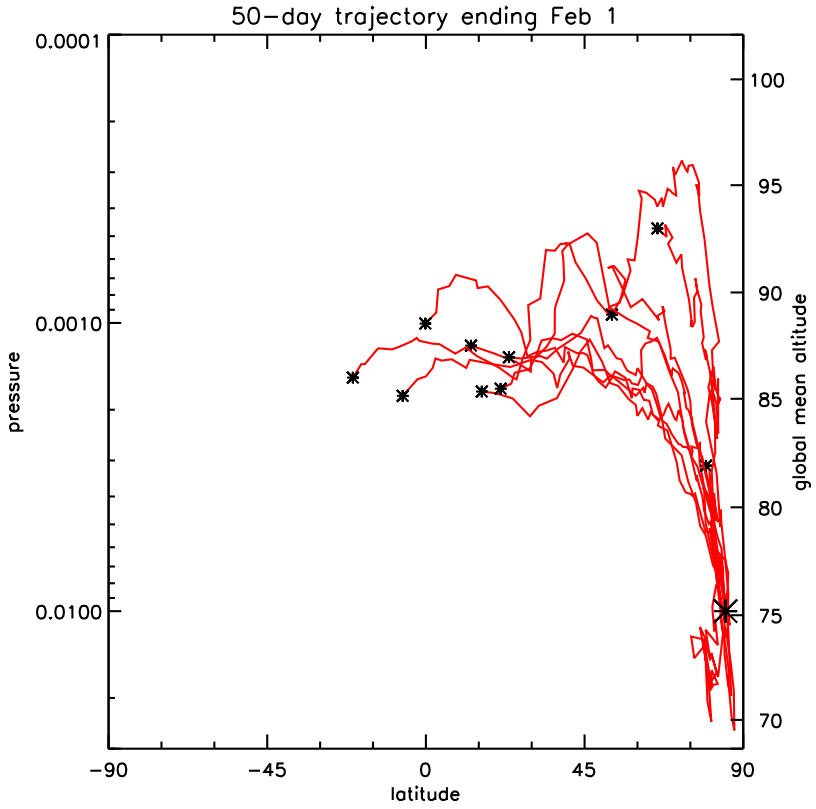

Figure 9. Trajectories of air parcels due to the TEM circulation for 50-day periods ending on February 1 at 85°N and 0.01 hPa for 10 years. The trajectory origins are marked by small asterisks. The large asterisk indicates the end location for all trajectories.

OH density in the polar night [*Damiani et al.*, 2010] and the reaction rate of OH with CO [*Sander et al.*, 2006], the maximum loss rate of CO is ~6×10^{-7} s^{-1}, or a lifetime of several weeks. The penetration of air with high CO into the winter middle atmosphere during the late winter of 2004, 2006, and 2009 that was documented by *Jin et al.* [2005], *Funke et al.* [2009], and *Damiani et al.* [2010] was an indication of unusual transport. During all three winters, a major stratospheric sudden warming was followed by a period with low planetary wave activity in the stratosphere, enhanced downwelling in the polar mesosphere, and a stratopause position much higher in altitude than normal. The unusual dynamics of those winters were confirmed by observations of temperature [*Manney et al.*, 2005, 2008, 2009] and were also seen in observed OH concentration [*Damiani et al.*, 2010] and airglow emissions [*Winick et al.*, 2009].

[45] Here we address the question of where the air parcels transported down near the winter pole have been prior to their descent. Figures 1 and 3 indicate that the circulation cell that is downward in the winter high latitudes extends only up to about 0.001 hPa (NH winter) or 0.0005 hPa (SH winter). Above that level, the mean circulation is upward although there is a weak downward motion over a very narrow region at the pole. Following the TEM streamlines (Figure 3), it appears that most of the air transported downward over the wide latitude band poleward of 60° originates in the middle atmosphere of the summer hemisphere.

[46] To determine more precisely the origin of the air, we use daily values of the TEM circulation, calculated using equations (9) and (10) from daily average model output. Coordinates of the end point (day, year, latitude and pressure) are specified and back trajectories give the origin point of the air parcel at a specified previous time. Figure 9 shows a sample of air parcel trajectories over a 50 day period ending on February 1 (i.e., trajectories beginning on 14 December of one year and ending on 1 February of the next). Trajectories for the years 1990–2000 from one of the model realizations are shown.

[47] Each trajectory in Figure 9 has an asterisk indicating the location at the start day of the 50 day period. Figure 10 shows those start positions only, and now includes trajectories for all four model realizations and for all years 1960 to 2006. The comparable plot for SH winter is also shown. It is evident from Figure 10 that, in mid-December, the majority of the air parcels were in the tropics or NH midlatitudes over a limited pressure range approximately 0.003 to 0.0005 hPa (~83–93 km). Only a handful of trajectories (5 out of 188) originate in the polar region at altitudes higher than 100 km. This distribution is consistent with the mean stream function during the NH winter; see the December average shown in Figure 3.

[48] Comparison of the NH and SH results in Figure 10 illustrates that the air parcels generally travel farther in SH winter due to the more vigorous circulation there. The parcels originating in low and middle latitudes generally

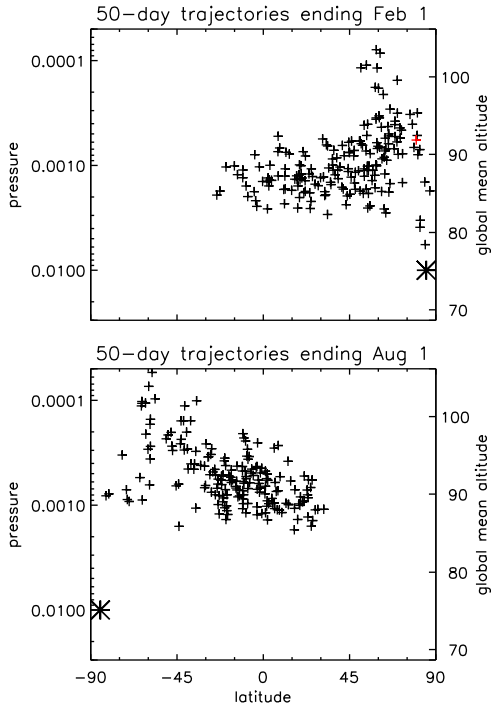

Figure 10. Points of origin (marked +) of 50-day air parcel trajectories due to the TEM circulation. Points are shown for the years 1960–2006 for four model runs. The end location for all trajectories is indicated by a large asterisk: (a) trajectories ending on February 1 at 85°N and 0.01 hPa; (b) trajectories ending on August 1 at 85°S and 0.01 hPa. The red + in Figure 10a (~92 km, 81°N) is for the case study described in section 5.

come from higher altitude than those in the NH, consistent with the mean circulation differences shown in Figure 1 and with the distribution of trace species in Figure 5. There are only a few years when air parcels are advected directly downward from the thermosphere into the middle atmosphere in either hemisphere. The trajectory origins illustrate that, for the WACCM climatology, descent of air in the polar region is slow (timescale of months) and that very few of the descending air parcels originate in the thermosphere.

[49] A look at the number of molecules involved shows the limitations of perturbations to the middle atmosphere by downward transport from the thermosphere. The number density n of air at pressure p is $n = p/(kT)$, where k is Boltzmann's constant. The total number of air molecules per unit area above p (i.e., the column amount) is $p/(kT) \cdot H$, where H is the atmospheric scale height. Using the definition $H = RT/g$, T can be eliminated from the expression for column amount. The air occupying the region poleward of latitude ϕ will have an areal extent proportional to $[1 - \sin(\phi)]$. Let n_{TOT} be the total number of molecules above p at latitudes poleward of ϕ. n_{TOT} depends on the latitude ϕ and pressure p as

$$n_{TOT} \propto [1 - \sin(\phi)] \cdot p\left(\frac{R}{k \cdot g}\right) \tag{15}$$

For a trace species with constant mixing ratio μ in the thermosphere, the total number of molecules in the same domain is $\mu \cdot n_{TOT}$. A volume of air from a higher pressure but having a lower mixing ratio can actually contain substantially more molecules of the trace species. Descending air can in principle draw from a wider latitude range, even from the entire globe. However, the impact of thermospheric molecules on the mixing ratios of a vortex-wide mass of air in the middle atmosphere is limited by the exponential decline of pressure with altitude.

[50] Applying numbers to equation (15) can give a sense of the magnitudes. Consider the global air mass above 0.0001 hPa (about 100 km), i.e. the entire global thermosphere. The global mean mixing ratio of NO at that level in WACCM is 3×10^{-5} (30 ppmv). We can estimate the mixing ratio that this same air would have if it were concentrated into the polar vortex but diluted in a higher density environment. Consider that the entire mass of the thermosphere is moved poleward to the NH polar vortex (60°N to the pole) and downward to 1 hPa (50 km) with no chemical loss. The resulting mixing ratio would be reduced by a factor of 0.0015, giving a mixing ratio of 45 ppbv. This mixing ratio is large but is nevertheless smaller than perturbations sometimes seen in NH winter. However, in this scenario, the air in the vortex contains a mix of thermospheric air and other air from the mesosphere. If the air transported from the upper mesosphere also contains high concentrations of NO_x, the NO mixing ratio at 1 hPa will be larger than the first estimate of 45 ppbv.

[51] The scenario for bringing down thermospheric air just discussed is an idealized case that does not account for chemical loss or additional dilution by lateral mixing across the vortex boundary. The scenario gives an upper limit for the concentration of NO_x in the polar vortex that has been transported by the mean circulation directly from the thermosphere. As pointed out elsewhere, eddy and molecular diffusion are quite important for the vertical transport of NO_x and other species, particularly above 90 km. In these model calculations, it is not possible to assess how much of the transport is due to the mean circulation alone and how much depends also on the diffusion. Future model tests are being planned to address this question.

5. Circulation and Trace Species Transport During an Active NH Winter

[52] This section illustrates the TEM circulation and tracer transport during a NH winter that was characterized by active dynamics. Recall that the model is free-running and so the calendar year does not necessarily resemble the same year in observations. The dynamical evolution during two different highly disturbed winters in WACCM are presented by *Chandran et al.* [2011] and *Limpasuvan et al.* [2011].

[53] *Funke et al.* [2009] and *Damiani et al.* [2010] presented observations of CO averaged over the NH polar region for several recent winters. These observations demonstrate that high concentrations of CO extend to higher pressure levels during dynamical events characterized by strong downwelling. The highest pressure of the 5 ppm contour shown by *Damiani et al.* [2010] for February–March 2006 and 2009 was about 0.3 hPa.

[54] Figure 11 shows the pressure of the 5 ppmv contour of CO from WACCM during the NH winter for the third realization, model year 2002, at daily intervals. The shading

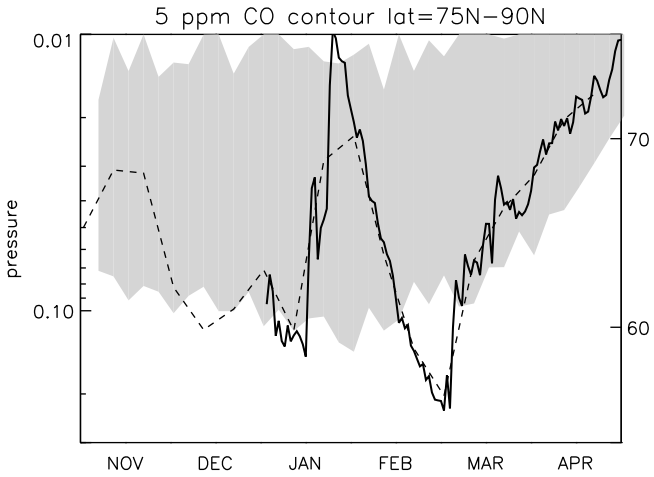

Figure 11. Pressure of the 5 ppmv contour of CO in the northern polar region for November through April. Data have been averaged over the latitudes 75°–90°N. The dashed black line gives the case for November 2001–April 2002 of the third model realization, determined from 10-day average data. The solid black line is for January–April 2002 of the same case, determined from daily data. The gray shaded area gives the range found in all other winters (187 cases) determined using 10-day average CO data.

shows the pressure range for all other NH winters using data at 10-day intervals (the normal output format). The maximum pressure of the 5 ppm contour during this winter is higher than that found in all the other winters from the four WACCM realizations analyzed here. The WACCM CO contours penetrate to 0.2 hPa, not quite as high a pressure (or equivalently as low an altitude) as seen during 2004 by *Funke et al.* [2009] and during 2006 and 2009 by *Damiani et al.* [2010].

[55] Cross-sections of the polar mean values of temperature, CO and NO_x for the same year are shown in Figure 12. NO_x is the sum of NO and NO_2. It behaves more like a tracer over the broader middle atmosphere as photochemical processes in the stratosphere and lower mesosphere convert rapidly between NO and NO_2. A major sudden stratospheric warming (SSW) occurred in the second half of January. The characteristic signature of this event can be seen in the high temperature in the middle stratosphere and low temperature above there in the lower and middle mesosphere. The simulated temperature behavior after the SSW is similar to the observed evolution during 2004, 2006, and 2009. Specifically, the altitude of the maximum temperature shifts abruptly to a much higher location, at about 80 km, and then descends over a period of weeks. This phenomenon has become known as the displaced or elevated stratopause.

[56] Figure 13 shows the TEM circulation for three days during 2002. Around the time of the SSW (23 January), the flow is strongly poleward in the stratosphere, with upwelling in the high latitude lower mesosphere. This circulation dies away quickly after the SSW (not shown) and is followed by a pattern more characteristic of a typical winter. The poleward flow in the upper mesosphere persists during February and early March (shown for 15 February and 8 March). The associated downwelling raises the temperature in the mesosphere and leads to the steady increase in the mixing ratios of CO and NO_x that are seen in Figure 12. Figure 14 shows a comparison between the February TEM climatological circulation at high northern latitudes and that for the perturbed year. During this dynamically active period, the mesospheric downwelling is stronger by about a factor of two than the climatological values. Note also that the poleward flow at high latitudes occurs at a lower altitude in the February 2002 simulation. The origin point of the 50-day back trajectory ending on February 1 of this period (the red symbol on Figure 10) is at high latitudes around 90 km.

[57] While the descent of CO in WACCM is similar to the observations during the most active years, the descent of NO_x in the model does not agree as well. *Randall et al.* [2009] show NO_x values that reach 100 ppbv at 60 km. For the year illustrated, concentrations above 100 ppbv are seen only above about 70 km. Recall that, by the measure of the 5 ppm CO contour, this is the strongest event we have seen in the free-running WACCM. Since this period occurred close to solar maximum, the NO concentrations in the MLT were higher than average. Nevertheless, the perturbation in WACCM falls short of that recently observed on several occasions, indicating a shortcoming of the free-running model. The limited penetration of high NO_x is also seen during other years with active dynamics (not shown). A similar discrepancy was seen in a WACCM integration adapted to simulate the 2005–2006 NH winter [*Marsh*, 2011]. In that case, the winds and temperatures in the troposphere and stratosphere were constrained to follow the observed evolution by nudging to analyzed global fields, while the dynamical evolution above 50 km was free-running.

[58] As discussed in section 4.3, comparison of WACCM simulations of H_2O and O with observations indicate discrepancies related to the mean circulation. A consistent interpretation of both comparisons implies that the altitude of the poleward component of the circulation in the NH winter in WACCM is too low. From the very strong vertical gradient of NO (Figure 5), an offset of a few kilometers can give up to a factor of 10 offset in the concentration of NO. This short-term discrepancy in the NO transport during the selected event illustrated in Figures 11–13 gives additional support for the concern that WACCM poleward flow during NH winter is occurring too low by several kilometers. Another contributing factor could be eddy diffusion rates that are too low in WACCM. As shown in Figure 8, eddy diffusion leads to an increase in the NO mixing ratio in the upper mesosphere during polar winter. If the diffusion rate is underestimated in WACCM, the downward diffusion of NO into the air parcels that subsequently descend near the pole will also be underestimated.

6. Conclusions

[59] Recent observations of NO, NO_2, CO, OH, and O have shown that the circulation near the winter pole can bring down air with higher concentrations of these tracers. The sharp increases in their concentrations during the periods following the sudden stratospheric warmings of late winter 2004, 2006, and/or 2009 were particularly noteworthy. The conventional understanding has been that these trace species, all of which have sources in the lower thermosphere,

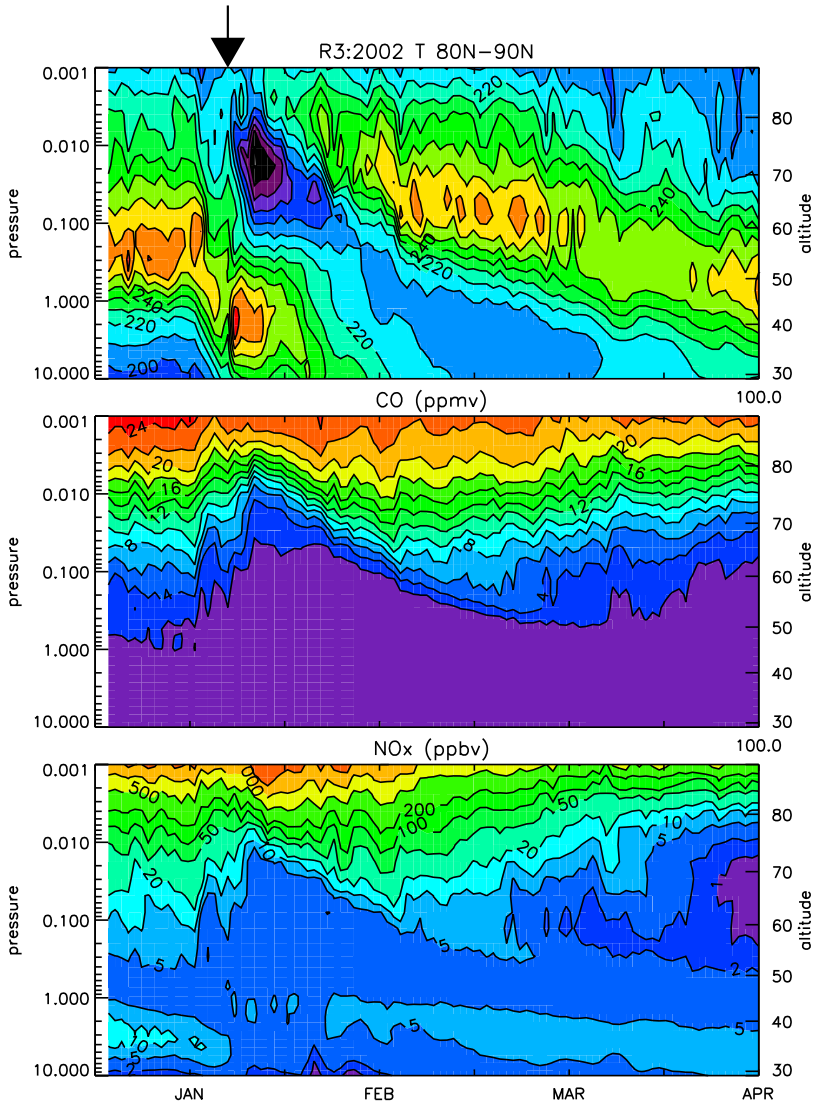

Figure 12. Pressure × day of year cross-sections of temperature, CO (ppmv) and NO_x (ppbv) mixing ratio for the first 100 days (1 January through 10 April) of the active NH winter 2002 of the third realization. Data have been averaged over the latitudes 80°–90°N. The arrow shows the onset of the sudden warming in the stratosphere.

represent the incursion of thermospheric air into the middle atmosphere.

[60] In the present study, we use the NCAR WACCM model to investigate transport in the mesosphere and its impact on trace species distributions. The model includes comprehensive interactive chemistry and dynamics of the atmosphere from the surface to about 140 km. The analysis primarily relies on monthly mean results from four integrations of the model over the period 1953–2006. The mass transport circulation is well represented by the two-dimensional transformed Eulerian mean (TEM) formulation introduced by *Andrews and McIntyre* [1976].

[61] The climatology of the TEM circulation in the solstice seasons is dominated by summer to winter flow in the upper mesosphere. Through mass continuity, this is accompanied by upwelling in the vicinity of the summer pole and downwelling in the vicinity of the winter pole. Above the altitude of strong meridional flow, there is another circulation cell with the opposite sense: upwelling near the winter pole and downwelling near the summer pole. The distributions of trace species with strong vertical gradients respond to these two circulation cells. Near the summer pole, where upwelling and downwelling motions converge, vertical gradients of CO_2, CO, O, and NO are much stronger than the global average. Vertical gradients of these species are weakest over the winter pole. Observations of water [*Lossow et al.*, 2009] and atomic oxygen confirm the basic sense of the circulation although some discrepancies remain.

[62] In WACCM, trajectories of air parcels following the TEM circulation indicate that, for the majority of winters, the air that is transported down in the late winter high latitudes does not originate in the thermosphere. Instead, air parcels are advected toward the winter pole from lower latitudes, following paths that are well predicted by the climatological TEM stream function. The multiyear mean

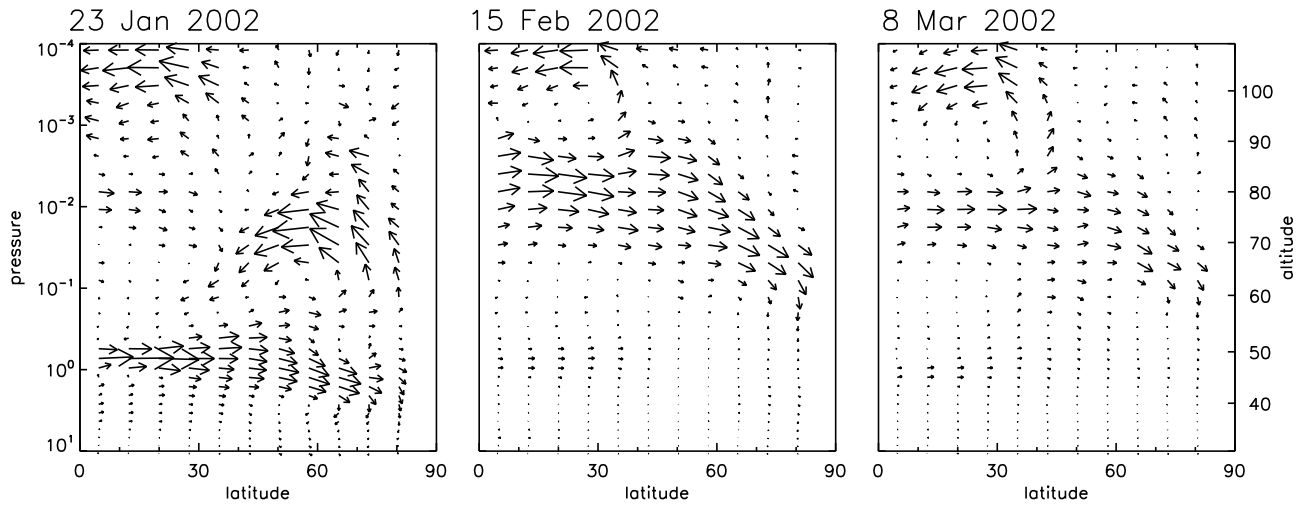

Figure 13. TEM vectors for the circulation for three days during the active NH winter 2002 of the third realization.

vertical motion has sinking at the winter pole below the altitude of poleward flow and rising above there, indicating that the air parcels are moving upward into the thermosphere. On the other hand, molecules of trace species can diffuse into or out of the air parcels through the action of molecular and eddy diffusion. So, while the air parcel itself has not been transported from the thermosphere, the bulk of the NO molecules, for example, could have been produced there.

[63] Advection in the winter middle atmosphere does bring down air that has higher concentrations of NO, NO_2, CO, and O, in agreement with the observations. The results confirm this downward transport and illustrate its hemispheric differences and interannual variability. The origin of the advected air, in low latitudes of the mesosphere rather than in the polar thermosphere, is a robust result in both hemispheres. 50-day back trajectories ending on 1 February (80°N) or on 1 August (80°S) give results that are representative of the winter advection. They indicate that the bulk of the air parcels originate in lower latitudes of the same hemisphere with origin altitudes centered at about 87 km (NH) or 92 km (SH). During a handful of winter seasons in both hemisphere, the air originated above 100 km in high latitudes.

[64] As noted above, the air mass transport represented by the TEM circulation is not the whole story for trace species. Vertical eddy and molecule diffusion can play a major role in the upper mesosphere. In the WACCM simulations analyzed here, the eddy diffusion coefficient peaks in the mesosphere and in general has a smaller impact on trace species distributions during solstice seasons than does the TEM circulation. However, molecular diffusion increases strongly with altitude and becomes a dominant process above ~90 km. Molecular diffusion that mixes individual molecules of a trace species downward, combined with the mean circulation governing air masses in the mesosphere, may be able to account for the perturbations to NO, CO and other trace species that have been observed during NH winter. It is likely that the combined effects of diffusion and advection by the mean circulation are sometimes more effective at changing the composition than the sum of their individual contributions. Both processes act to increase the

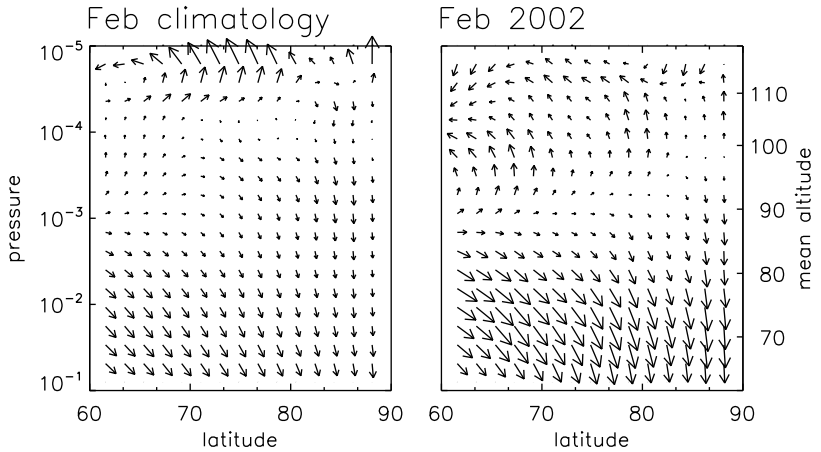

Figure 14. February mean TEM vectors in the NH for the WACCM climatology and the active NH winter 2002 of the third realization.

mixing ratios of NO and O in the polar winter but the altitudes where they are most effective are offset. Together, the altitude range over which dynamical processes perturb the chemical composition is broader. Additional model runs with the capability of distinguishing the relative roles of diffusive processes and advection by the TEM circulation are needed to determine a quantitative breakdown of the roles of these processes.

[65] The TEM circulation is difficult to determine from mesospheric observations of dynamical fields. The best approach for verifying the WACCM simulations is comparison of the simulated trace species distributions with observations. The comparisons discussed here indicate that WACCM simulations cannot reproduce all of the details of the observations. We note two discrepancies (possibly related) in particular. First, in the NH, the altitude of the transition from summer maximum to winter maximum for H_2O and vice versa for O is too low in WACCM. This suggests that the altitude of the peak of the gravity wave driving of the circulation is too low. The equivalent transitions in the SH, on the other hand, are well simulated. The second discrepancy is that the amount of NO that descends into the lower mesosphere and stratosphere during the most extreme dynamical events falls short of that observed. Results from one winter were presented but the NO descent during other active winters was similar. This difference could also be affected by the vertical extent of the poleward winter circulation. If the altitude of the poleward flow is too low, the NO increases by diffusion or chemical processes will be underestimated in the simulation. However, a simulated eddy diffusion due to gravity waves that is too weak could also cause or contribute to the discrepancy.

[66] **Acknowledgments.** The National Center for Atmospheric Research is sponsored by the National Science Foundation. Support for this work was also provided by the NASA Heliospheric Guest Investigator Program.

References

Andrews, D. G., and M. E. McIntyre (1976), Planetary waves in horizontal and vertical shear: The generalized Eliassen-Palm relation and mean zonal acceleration, *J. Atmos. Sci.*, *33*, 2031–2048.

Banks, P. M., and G. Kockarts (1973), *Aeronomy: Part B*, Academic, San Diego, Calif.

Beagley, S. R., C. D. Boone, V. I. Fomichev, J. J. Jin, K. Semeniuk, J. C. McConnell, and P. F. Bernath (2010), First multi-year occultation observations of CO_2 in the MLT by ACE satellite: Observations and analysis using the extended CMAM, *Atmos. Chem. Phys.*, *10*, 1133–1153.

Chandran, A., R. L. Collins, R. R. Garcia, and D. R. Marsh (2011), A case study of an elevated stratopause generated in the Whole Atmosphere Community Climate Model, *Geophys. Res. Lett.*, *38*, L08804, doi:10.1029/2010GL046566.

Damiani, A., M. Storini, M. L. Santee, and S. Wang (2010), Variability of the nighttime OH layer and mesospheric ozone at high latitudes during northern winter: Influence of meteorology, *Atmos. Chem. Phys.*, *10*, 10,291–10,303.

Eyring, V., et al. (2006), Assessment of temperature, trace species and ozone in chemistry-climate simulations of the recent past, *J. Geophys. Res.*, *111*, D22308, doi:10.1029/2006JD007327.

Eyring, V., T. G. Shepherd, and D. W. Waugh (Eds.) (2010), *SPARC Report on the Evaluation of Chemistry-Climate Models*, *WCRP-132, WMO/TD-No.1526*, World Clim. Res. Programme, Geneva, Switzerland.

Funke, B., et al. (2009), Carbon monoxide distributions from the upper troposphere to the mesosphere inferred from 4.7 μm non-local thermal equilibrium emissions measured by MIPAS on Envisat, *Atmos. Chem. Phys.*, *9*, 2387–2411.

Garcia, R. R., and S. Solomon (1983), A numerical model of the zonally averaged dynamical and chemical structure of the middle atmosphere, *J. Geophys. Res.*, *88*, 1379–1400.

Garcia, R. R., D. R. Marsh, D. E. Kinnison, B. A. Boville, and F. Sassi (2007), Simulation of secular trends in the middle atmosphere, 1950–2003, *J. Geophys. Res.*, *112*, D09301, doi:10.1029/2006JD007485.

Gent, P. R., S. G. Yeager, R. B. Neale, S. Levis, and D. A. Bailey (2009), Improvements in a half degree atmosphere/land version of the CCSM, *Clim. Dyn.*, *34*, 819–833, doi:10.1007/s00382-009-0614-8.

Hauchecorne, A., J.-L. Bertaux, F. Dalaudier, J. M. Russell, M. G. Mlynczak, E. Kyrölä, and D. Fussen (2007), Large increase of NO_2 in the north polar mesosphere in January-February 2004: Evidence of a dynamical origin from GOMOS/ENVISAT and SABER/TIMED data, *Geophys. Res. Lett.*, *34*, L03810, doi:10.1029/2006GL027628.

Huang, Y. W. T., and A. K. Smith (1991), The mesospheric diabatic circulation and a comparison of the momentum residual and parameterized gravity wave drag, *J. Atmos. Sci.*, *48*, 1093–1111.

Jin, J. J., et al. (2005), Co-located ACE-FTS and Odin/SMR stratospheric-mesospheric CO 2004 measurements and comparison with a GCM, *Geophys. Res. Lett.*, *32*, L15S03, doi:10.1029/2005GL022433.

Lieberman, R. S., et al. (2000), Comparison of mesospheric and lower thermospheric residual wind with High Resolution Doppler Imager, medium frequency, and meteor radar winds, *J. Geophys. Res.*, *105*, 27,023–27,035.

Limpasuvan, V., J. H. Richter, Y. J. Orsolini, F. Stordal, and Ole-KristianKvissel (2011), The roles of planetary and gravity waves during a major stratospheric sudden warming as characterized in WACCM, *J. Atmos. Sol. Terr. Phys.*, *73*, doi:10.1016/j.jastp.2011.03.004.

López Puertas, M., M. A. López Valverde, R. R. Garcia, and R. G. Roble (2000), A review of CO_2 and CO abundances in the middle atmosphere, in *Atmospheric Science Across the Stratopause*, *Geophys. Monogr. Ser.*, vol. 123, edited by D. E. Siskind, S. D. Eckermann, and M. E. Summers, pp. 83–100, AGU, Washington, D. C.

López-Puertas, M., B. Funke, S. Gil-López, T. von Clarmann, G. P. Stiller, M. Höpfner, S. Kellmann, H. Fischer, and C. H. Jackman (2005), Observation of NO_x enhancement and ozone depletion in the Northern and Southern hemispheres after the October–November 2003 solar proton events, *J. Geophys. Res.*, *110*, A09S43, doi:10.1029/2005JA011050.

Lossow, S., J. Urban, H. Schmidt, D. R. Marsh, J. Gumbel, P. Eriksson, and D. Murtagh (2009), Wintertime water vapor in the polar upper mesosphere and lower thermosphere: First satellite observations by Odin submillimeter radiometer, *J. Geophys. Res.*, *114*, D10304, doi:10.1029/2008JD011462.

Manney, G. L., K. Krüger, J. L. Sabutis, S. Amina Sena, and S. Pawson (2005), The remarkable 2003–2004 winter and other recent warm winters in the Arctic stratosphere in the late 1990s, *J. Geophys. Res.*, *110*, D04107, doi:10.1029/2004JD005367.

Manney, G. L., et al. (2008), The evolution of the stratopause during the 2006 major warming: Satellite data and assimilated meteorological analyses, *J. Geophys. Res.*, *113*, D11115, doi:10.1029/2007JD009097.

Manney, G. L., M. J. Schwartz, K. Krüger, M. L. Santee, S. Pawson, J. N. Lee, W. H. Daffer, R. A. Fuller, and N. J. Livesey (2009), Aura microwave limb sounder observations of dynamics and transport during the record-breaking 2009 Arctic stratospheric major warming, *Geophys. Res. Lett.*, *36*, L12815, doi:10.1029/2009GL038586.

Marsh, D., and R. Roble (2002), TIME-GCM simulations of lower-thermospheric nitric oxide seen by the halogen occultation experiment, *J. Atmos. Solar Terr. Phys.*, *64*, 889–895.

Marsh, D., R. R. Garcia, D. E. Kinnison, B. A. Bouville, F. Sassi, S. C. Solomon, and K. Matthes (2007), Modeling the whole atmosphere response to solar cycle changes in radiative and geomagnetic forcing, *J. Geophys. Res.*, *112*, D23306, doi:10.1029/2006JD008306.

Marsh, D. R. (2011), Chemical-dynamical coupling in the mesosphere and lower thermosphere, in *Aeronomy of the Earth*'s *Atmosphere and Ionosphere*, *IAGA Spec. Sopron Book Ser.*, vol. 2, edited by M. Abdu, D. Pancheva, and A. Bhattacharyya, pp. 3–17, Springer, Dordrecht, Netherlands.

Minschwaner, K., et al. (2010), The photochemistry of carbon monoxide in the stratosphere and mesosphere evaluated from observations by the Microwave Limb Sounder on the Aura satellite, *J. Geophys. Res.*, *115*, D13303, doi:10.1029/2009JD012654.

Randall, C. E., V. L. Harvey, C. S. Singleton, P. F. Bernath, C. D. Boone, and J. U. Kozyra (2006), Enhanced NO_x in 2006 linked to strong upper stratospheric Arctic vortex, *Geophys. Res. Lett.*, L18811, doi:10.1029/2006GL027160.

Randall, C. E., V. L. Harvey, C. S. Singleton, S. M. Bailey, P. F. Bernath, M. Codrescu, H. Nakajima, and J. M. R. III (2007), Energetic particle precipitation effects on the Southern Hemisphere stratosphere in 1992–2005, *J. Geophys. Res.*, *112*, D08308, doi:10.1029/2006JD007696.

Randall, C. E., V. L. Harvey, C. S. Singleton, P. F. Bernath, C. D. Boone, and K. A. Walker (2009), NO_x descent in the Arctic middle atmosphere in early 2009, *Geophys. Res. Lett.*, *36*, L18811, doi:10.1029/2009GL039706.

Richter, J. H., F. Sassi, and R. R. Garcia (2010), Towards a physically based gravity wave source parameterization in a general circulation model, *J. Atmos. Sci.*, *67*, 136–156.

Sander, S. P., et al. (2006), Chemical kinetics and photochemical data for use in atmospheric studies, *JPL Publ. 06-2*, Jet Propul. Lab., Pasadena, Calif.

Siskind, D. E., J. T. Bacmeister, and M. E. Summers (1997), Two-dimensional model calculations of nitric oxide transport in the middle atmosphere and comparison with Halogen Occultation Experiment data, *J. Geophys. Res.*, *102*, 3527–3545.

Siskind, D. E., S. D. Eckermann, J. P. McCormack, M. J. Alexander, and J. T. Bacmeister (2003), Hemispheric differences in the temperature of the summertime stratosphere and mesosphere, *J. Geophys. Res.*, *108*(D2), 4051, doi:10.1029/2002JD002095.

Smith, A. K., and D. R. Marsh (2005), Processes that account for the ozone maximum at the mesopause, *J. Geophys. Res.*, *110*, D23305, doi:10.1029/2005JD006298.

Smith, A. K., M. Lopéz-Puertas, M. García-Comas, and S. Tukiainen (2009), SABER observations of mesospheric ozone during NH late winter 2002–2009, *Geophys. Res. Lett.*, *36*, L23804, doi:10.1029/2009GL040942.

Smith, A. K., D. R. Marsh, M. G. Mlynczak, and J. C. Mast (2010a), Temporal variations of atomic oxygen in the upper mesosphere from SABER, *J. Geophys. Res.*, *115*, D18309, doi:10.1029/2009JD013434.

Smith, A. K., R. R. Garcia, D. R. Marsh, D. E. Kinnison, and J. H. Richter (2010b), Simulations of the response of mesospheric circulation and temperature to the Antarctic ozone hole, *Geophys. Res. Lett.*, *37*, L22803, doi:10.1029/2010GL045255.

Winick, J. R., P. P. Wintersteiner, R. H. Picard, D. Esplin, M. G. Mlynczak, J. M. Russell III, and L. L. Gordley (2009), OH layer characteristics during unusual boreal winters of 2004 and 2006, *J. Geophys. Res.*, *114*, A02303, doi:10.1029/2008JA013688.

World Meteorological Organization (2010), Scientific assessment of ozone depletion: 2010, *Rep. 52*, Global Ozone Res. and Monit. Proj., Geneva, Switzerland.

R. R. Garcia, D. R. Marsh, and A. K. Smith, Atmospheric Chemistry Division, National Center for Atmospheric Research, PO Box 3000, Boulder, CO 80307, USA. (aksmith@ucar.edu)

J. H. Richter, Climate and Global Dynamics, National Center for Atmospheric Research, PO Box 3000, Boulder, CO 80307, USA.